CrossMark

A facile colloidal crystal templating method to produce three-dimensional hierarchical porous graphene–Fe$_3$O$_4$ nanocomposite for the removal of dyes from aqueous solution

Yurong Liu[1] · Rong Hu[1] · Zongqiang Zhang[1]

Abstract

Three-dimensional hierarchical porous graphene–Fe$_3$O$_4$ (3D-HPGF) nanocomposite was synthesized through a facile colloidal crystal templating method and used as adsorbent for the removal of organic dyes from aqueous solution. The obtained 3D-HPGF nanocomposite had high specific surface area and three-dimensional hierarchical porous structure. The adsorption behaviors of 3D-HPGF nanocomposite for methylene blue dye in aqueous solution were systematically investigated. Results showed that 3D-HPGF nanocomposite adsorbent exhibited extraordinary adsorption capacities and fast adsorption rates for the removal of organic dye. The excellent adsorption capacities of 3D-HPGF nanocomposite could be attributed to the van der Waals interactions and strong π–π interactions between graphene and organic dye. The kinetics and equilibrium adsorptions were well-described by pseudo-second-order kinetic and Langmuir isotherm model, respectively. The thermodynamic parameters revealed that the adsorption process was spontaneous and endothermic in nature. In addition, 3D-HPGF nanocomposite could be easily regenerated for reuse through magnetic separation and ethanol treatment. Due to the excellent adsorption capacity, fast adsorption rate and convenient magnetic separation, the as-prepared 3D-HPGF nanocomposite could be utilized as an efficient, magnetically separable adsorbent for the environmental applications.

1 Introduction

With the rapid development of global economy, industries based on cosmetic, rubber, tanning, food, plastic, pharmaceutical, paper and textile use very large amount of dyes, and the waste from these industries is a major environmental concern [1]. So, it is highly desired to develop eco-friendly, simple and economical techniques for the removal of hazardous dyes from wastewater [2]. To date, several methods have been developed for the removal of dye pollutants, such as degradation, membrane separation and chemical oxidation, and so on [3–5]. However, some of these techniques have some disadvantages, for instance, high cost, high energy requirements, incomplete removal and production of toxic sludge [6]. Compared with the above methods, adsorption is a promising water-treatment technology due to its low invest-cost, simplicity of design and operation, no discharge of harmful substances, high efficiency and availability of a wide range of adsorbents [7–9]. The commonly used adsorbents primarily include activated carbons [10], carbon xerogels [11], carbon nanofibers [12], nanomaterials [13–15] and polymer sorbents [16, 17]. Although these types of adsorbents have shown promise in treating wastewater, some limitations still exist, such as low adsorption capacities and separation inconveniences. Therefore, the exploration of new promising adsorbents for the removal of dyes is still necessary.

Graphene is a new type of two-dimensional carbon nanostructure with one-atom thickness, possessing large surface area and good chemical stability [18]. Moreover, the graphitized basal plane structure of graphene has strong π–π interactions with the aromatic moieties of dyes [19]. These advantages reveal that graphene can be a promising material

✉ Yurong Liu
liuyr1978@163.com

1 Research Institute for New Materials Technology, College of Materials and Chemical Engineering, Chongqing University of Arts and Sciences, Chongqing 402160, People's Republic of China

for the environmental cleanup, especially for the removal of dye pollutants from aqueous solution [20–27]. However, the two-dimensional lamellar structure of graphene is easily distorted into other uncontrolled morphologies, leading to a sharp decline in performance [28]. Therefore, it is of great significance to develop an efficient and facile strategy to transform two-dimensional graphene nanosheets into three-dimensional graphene networks with controlled morphology and porous structures [29–33]. On the other hand, it is very difficult to separate graphene from aqueous solution even by high-speed centrifugation because of its small size. Therefore, developing adsorbents which combine the advantages of high surface area of graphene with separation convenience of magnetic materials will be very important and urgent for the removal of toxic pollutants from wastewater [34–39].

However, there are few works about the synthesis of magnetic graphene-based adsorbents with controlled morphology and porous structures for environmental applications [40]. In the present work, three-dimensional hierarchical porous graphene–Fe_3O_4 (3D-HPGF) nanocomposite has been fabricated by poly(methyl methacrylate) (PMMA) colloidal crystal templating method. The potential practical application of 3D-HPGF nanocomposite for the removal of organic dyes from aqueous solution has been investigated systematically.

2 Experimental

2.1 Materials

Carboxylic graphene oxide (GO-COOH) aqueous solution was purchased from Nanjing XFNANO Materials Tech Co., Ltd, China. Ferrous sulfate ($FeSO_4·7H_2O$), methylene blue (MB), sodium hydroxide (NaOH), hydrochloric acid (HCl), Pyromellitic dinahydride anhydride (PMDA), 4, 40-diamino diphenyl ether (ODA, AR) and 1-methyl-2-pyrrolidone (NMP) of analytical grade were purchased from Sinopharm Chemical Reagent Co. Ltd., China. PMDA and ODA were recrystallized from acetic anhydride and ethanol before use, respectively. NMP was distilled over phosphorus pentoxide before use. Ultrapure water was used throughout the experiment.

2.2 Synthesis of PMMA colloidal crystal templates

PMMA microspheres were synthesized by surfactant-free emulsion polymerization using a cationic free radical initiator, as described in a previous report [41]. The synthesized PMMA microspheres were positively charged in aqueous solutions and the concentration of colloidal solution used here was 1.0 wt%. PMMA colloidal crystals were formed by centrifuging the colloid at 1500 rpm for 24 h, decanting the

water, and allowing the solid to dry for 3 days. Before being used as templates, the PMMA colloidal crystal pellets were crushed with a metal spatula to form powder [42].

2.3 Preparation of 3D-HPGF nanocomposite

3D-HPGF nanocomposite was fabricated through PMMA colloidal crystal templating method. In a typical synthesis procedure, 1.0 g of dried PMMA colloidal crystals were crushed into powder and deposited in millimeter-thick layers. 50 mL of GO-COOH dispersion (1 mg/mL) was applied dropwise to completely wet the PMMA powder. The sample was allowed to dry in air at room temperature for 3 days. Then 20 mL of $FeSO_4·7H_2O$ aqueous solution (0.3 mol/L) was added dropwise into the mixture followed by air drying for another 3 days. The PMMA template was removed from the sample by calcination at 600 °C for 3 h under nitrogen atmosphere.

2.4 Characterization

X-ray diffraction (XRD) measurements were carried out using a Rigaku SmartLab X-ray diffractometer at 40 kV, 30 mA. The morphology and structure of samples were observed by scanning electron microscopy (SEM) using a Hitachi S-3400N electron microscope operated at 20 kV and transmission electron microscopy (TEM) using a JEOL model JEM-2011(HR) with an accelerating voltage of 200 kV. X-ray photoelectron spectroscopy (XPS) measurements were performed on an ESCALAB 250 analyzer (Thermo Scientific) with a monochromatic Al Ka (1486.8 eV photons) X-ray source for excitation. Brunauer–Emmett–Teller (BET) surface area and pore size distribution were measured by Tristar-3020 surface area analyzer.

2.5 Adsorption of MB dye onto 3D-HPGF nanocomposite

The adsorption of MB dye in aqueous solution by using the as-prepared 3D-HPGF nanocomposite was performed in a batch experiment. 10 mg of 3D-HPGF nanocomposite adsorbent was added into 25 mL of MB solutions of desired initial concentrations (10, 20, 30, 40, 50, 60 mg/L) under stirring. At predetermined time intervals (10, 25, 35, 45, 60, 80, 100 min), 3D-HPGF nanocomposite adsorbent was separated from aqueous solution by a permanent magnet. The effect of temperature on the adsorption of MB dye onto the composite adsorbent was investigated by determining the adsorption isotherms at 298, 308 and 318 K. The concentrations of dyes were determined by UV-2450 Ultraviolet–Visible spectrophotometer. The amount of MB dye adsorbed per

unit mass of the adsorbent was evaluated by the following equation:

$$q = \frac{(C_0 - C_e)V}{m} \tag{1}$$

where q (mg/g) is the amount adsorbed per unit mass, C_0 and C_e are the initial and equilibrium concentrations of MB dye in the solution (mg/L), respectively, m is the mass of the adsorbent used (g), and V (L) is the initial volume of solution.

2.6 Desorption and regeneration experiments

For the desorption study, 10 mg of 3D-HPGF nanocomposite adsorbent was added into 25 mL of MB dye solution (30 mg/L) and the mixture was stirred for 30 min at ambient temperature. After magnetic separation, the supernatant dye solution was discarded and the adsorbent alone was separated. Then, the MB-adsorbed adsorbent was added into 25 mL of ethanol and stirred for 30 min. The adsorbent was collected by magnet and reused for adsorption again. The supernatant solutions were analyzed by Ultraviolet–Visible spectrophotometer. The cycles of adsorption–desorption processes were successively conducted five times.

3 Results and discussion

3.1 Characterization of 3D-HPGF nanocomposite

X-ray diffraction measurements were utilized to investigate the phase and structure of samples. In the representative XRD pattern of 3D-HPGF nanocomposite (Fig. 1), the different peaks at $2\theta = 18.5°$, 30.1°, 35.5°, 37.1°, 43.6°, 53.3°, 57.0°, 62.8°, 71.1° and 73.9° are observed. These diffraction peaks can be assigned to (111), (220), (311), (222), (400), (422), (511), (440), (620) and (533) planes of Fe_3O_4 (JCPDS no. 89-3854) [43]. The broad peak at $2\theta = 26.2°$ originates from (002) reflection of graphene. No obvious diffraction peak ascribed to GO is observed, indicating that GO has been successfully reduced into graphene.
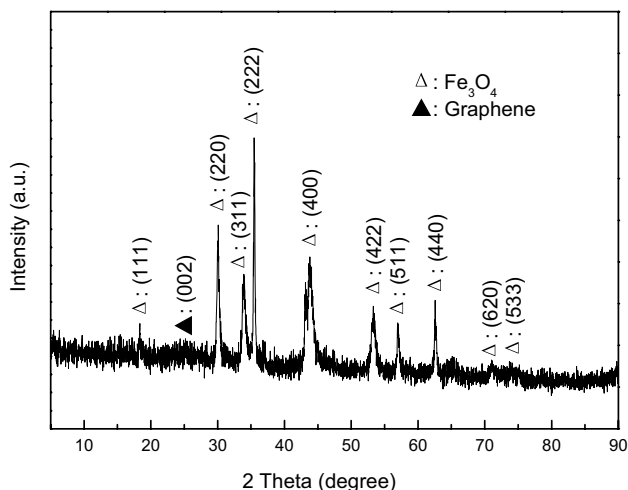
Detailed information about the composition of samples was examined by X-ray photoelectron spectroscopy measurements. The sharp peaks at about 284, 534 and 711 eV in the full scan spectrum (Fig. 2a) are corresponding to the C1s, O1s and Fe2p, respectively, revealing the presence of carbon, oxygen, and iron elements in 3D-HPGF nanocomposite. Four different peaks centered at 284.8, 286.1, 287.1, and 288.5 eV are observed in the C1s spectrum, corresponding to C=C, C–C in aromatic rings, C–OH (epoxy and alkoxy), and C=O groups, respectively (Fig. 2b), demonstrating the removal of oxygen-containing groups from GO and the formation of graphene [44, 45]. In the Fe2p spectrum (Fig. 2c), the two peaks at 711.2 and 724.6 eV are corresponding to $Fe2p_{3/2}$ and $Fe2p_{1/2}$ of Fe_3O_4, respectively [46]. This can be further supported by the peak at 530.2 eV in the O1s spectrum (Fig. 2d), which is the binding energy of crystal oxygen in Fe_3O_4. Other peaks located at 531.8 and 533.7 eV can be attributed to the carbonyl oxygen in C=O and the oxygen in C–O.

SEM was employed to investigate the morphology and structure of samples. Figure 3a shows SEM image of typical core/shell microsphere assembly of cationic PMMA microspheres and negative GO-COOH nanosheets. It can be clearly seen that GO nanosheets coating onto the PMMA microshperes. Figure 3b shows the SEM image of as-prepared 3D-HPGF nanocomposite. The spherical macropores with a pore size of about 200–250 nm can be clearly observed and the spherical PMMA structures have disappeared. These macropores are composed of aggregated graphene nanosheets, forming a three-dimensional porous structure.

The morphology and structure of samples were further analyzed by TEM measurements. It can be seen that Fe_3O_4 nanoparticles with an average size of 20 nm are well distributed on the surface of graphene nanosheets (Fig. 4a). The distribution of Fe_3O_4 nanoparticles on each graphene sheet is uniform and no big conglomeration is observed. HRTEM image of 3D-HPGF nanocomposite reveals clear lattice fringes with an interplanar distance of 0.257 nm, which agrees well with the basal spacing of cubic Fe_3O_4 (Fig. 4b) [47]. In addition, the ordered graphitic lattices are visible in the HRTEM image of 3D-HPGF nanocomposite.

Nitrogen adsorption–desorption isotherms and pore size distributions of 3D-HPGF nanocomposite are shown in Fig. 5. The sharp steps at the relative pressure around $P/P_0 = 0.5$ is associated with capillary condensation of nitrogen molecules

**Fig. 1** XRD pattern of 3D-HPGF nanocomposite
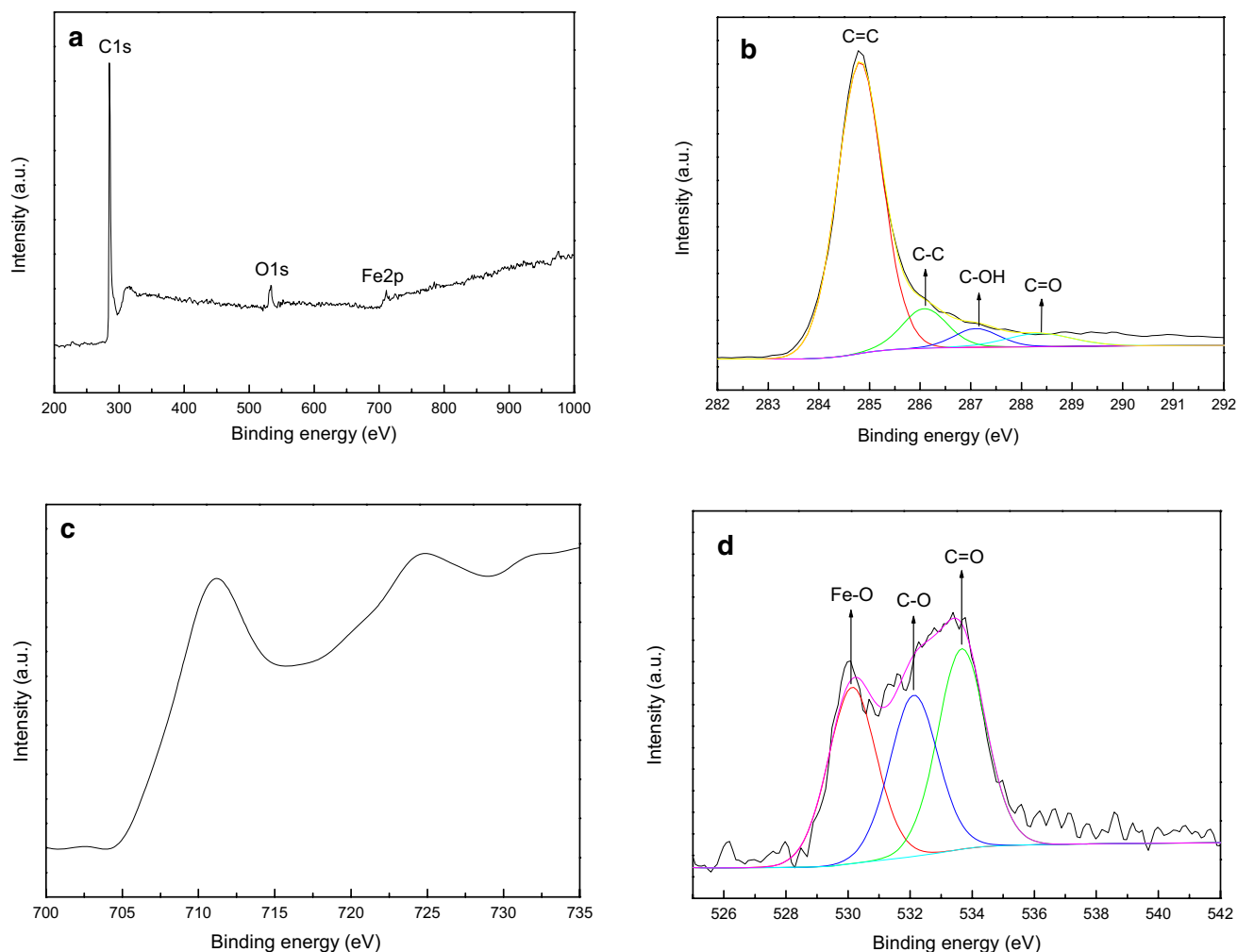
Fig. 2 XPS spectra of 3D-HPGF nanocomposite. **a** XPS survey spectrum, **b** C1s spectrum (The black lines are raw data and the colorful lines are fitted data), **c** Fe2p spectrum, **d** O1s spectrum (The black lines are raw data and the colorful lines are fitted data)

inside the pores. The BET specific surface area of 3D-HPGF nanocomposite is 486 m^2/g. The large specific surface area can be attributed to the presence of Fe$_3$O$_4$ nanoparticles preventing the aggregation and restacking of graphene nanosheets, owing to the spacing effect of magnetite nanoparticles between graphene nanosheets [48]. The pore size distribution curve of 3D-HPGF nanocomposite exhibits typical bimodal mesopores with small mesopores of about 3.0 nm and large mesopores of about 14.9 nm. Therefore, combined with SEM and TEM measurements, the 3D-HPGF nanocomposite has a hierarchical porous structure with interconnected macro- and mesopores. The large specific surface area and hierarchical porous structure will guarantee the adsorption performance of

3D-HPGF nanocomposite for removing the dye contaminants from wastewater.

3.2 Adsorption properties of 3D-HPGF nanocomposite

The effects of contact time on the adsorption of MB dye onto 3D-HPGF nanocomposite adsorbent are shown in Fig. 6. It can be seen that the adsorption capacity increases sharply with the contact time, and the contact time to reach the equilibrium is about 25 min. And the amount of adsorbed MB dye on the 3D-HPGF nanocomposite achieves 69.6 mg/g. The excellent adsorption capacity and fast adsorption rate
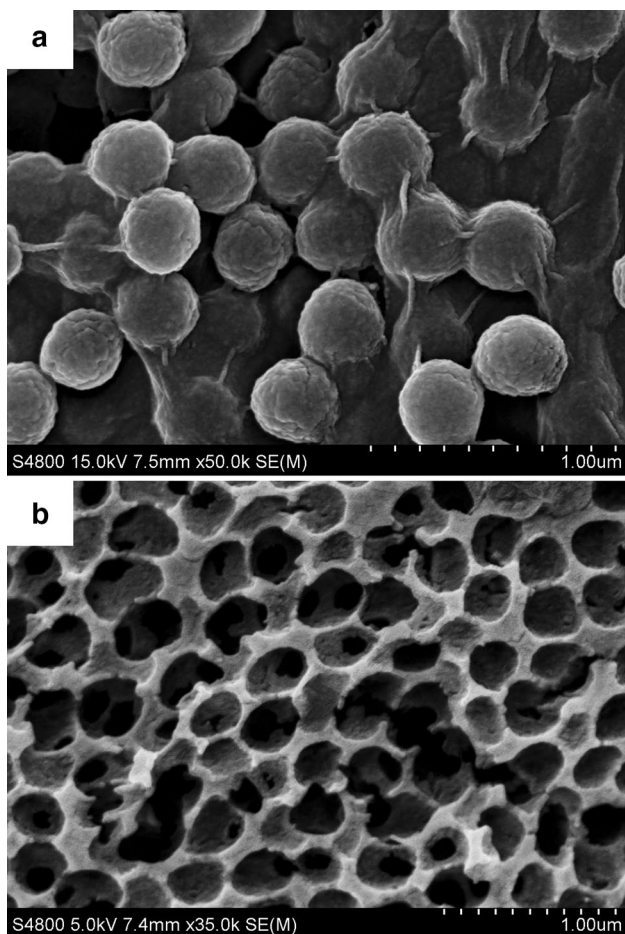
Fig. 3 SEM images of **a** PMMA/GO-COOH microspheres, **b** 3D-HPGF nanocomposite

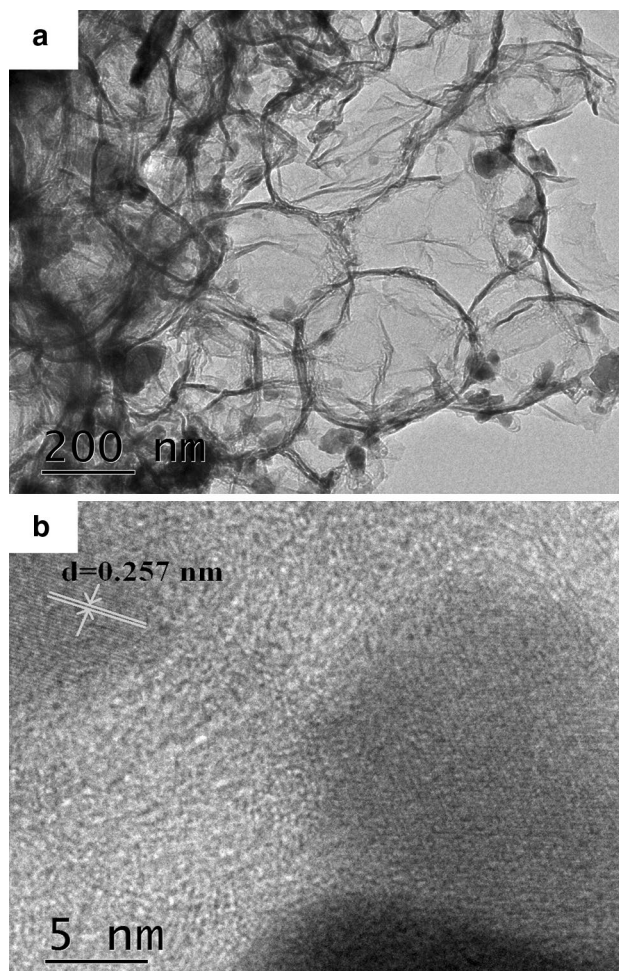**Fig. 4** TEM (**a**) and HRTEM (**b**) images of 3D-HPGF nanocomposite

of 3D-HPGF nanocomposite for organic dye can be attributed to the van der Waals interactions occurring between the hexagonally arrayed carbon atoms in the graphene nanosheet and the aromatic backbones of organic dye, and the strong π–π interactions between the benzene ring of MB dye and the large delocalized π-electron system of graphene [49].

To further investigate the adsorption behavior of MB dye onto 3D-HPGF nanocomposite adsorbent, the kinetic data are evaluated by pseudo-first-order and pseudo-second-order adsorption kinetic model, which can be expressed by the following equations.

$$\log(q_e - q_t) = \log q_e - \frac{k_1 t}{2.303} \tag{2}$$

$$\frac{t}{q_t} = \frac{1}{k_2 q_e{}^2} + \frac{t}{q_e} \tag{3}$$

Here k_1 (min^{-1}) and k_2 (g/mg min) are the rate constant for pseudo-first-order and pseudo-second-order adsorption

kinetics, respectively. q_e and q_t are the amounts of MB dye adsorbed (mg/g) at equilibrium and time t (min), respectively.

Figure 7a indicates the linear dependence between $\log(q_e - q_t)$ and t, where the values of k_1 and q_e can be determined from the intercept and slope of the plot. Meanwhile, k_2 and q_e can be calculated by the intercept and slope of the linear plot t/q_t vs. t in Fig. 7b. The corresponding kinetic parameters are listed in Table 1. Obviously, the correlation coefficient R^2 calculated by pseudo-first-order is smaller than that of pseudo-second-order model. It means that the pseudo-second-order model is more suitable to describe the adsorption kinetics of 3D-HPGF nanocomposite adsorbent for MB dye.

Adsorption isotherms can afford the useful information for designing a desired adsorption system. The adsorption performance of 3D-HPGF nanocomposite adsorbent is evaluated by the classical Langmuir model and Freundlich model. The Langmuir isotherm is usually utilized to a homogeneous adsorption surface with all the adsorption
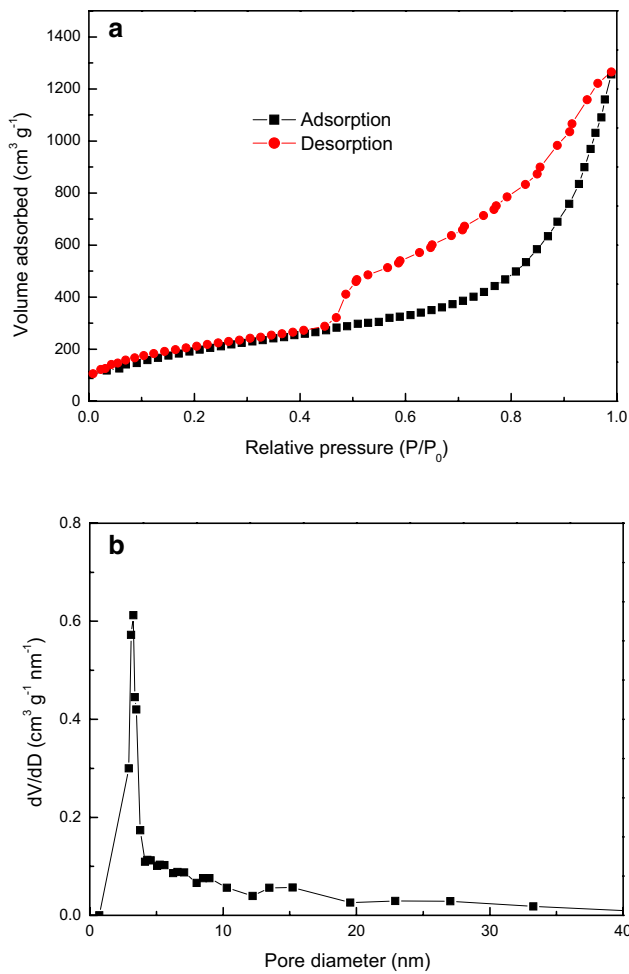
Fig. 5 Nitrogen adsorption–desorption isotherms (**a**) and pore size distributions (**b**) of 3D-HPGF nanocomposite
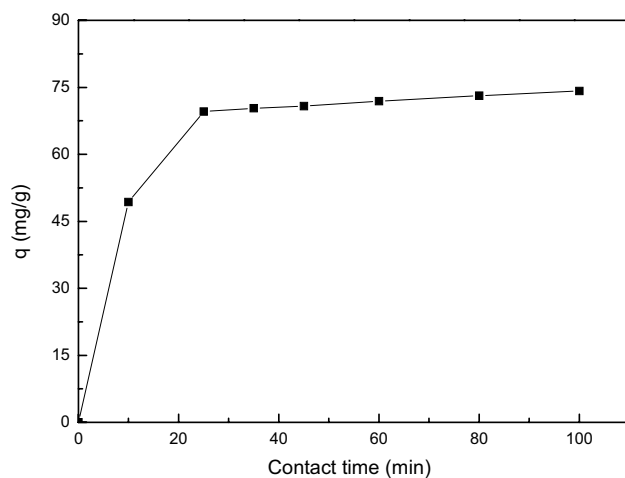
Fig. 6 Effects of contact time on the adsorption capacities of 3D-HPGF nanocomposite adsorbent (pH 6, initial dye concentration = 30 mg/L, T = 298 K)
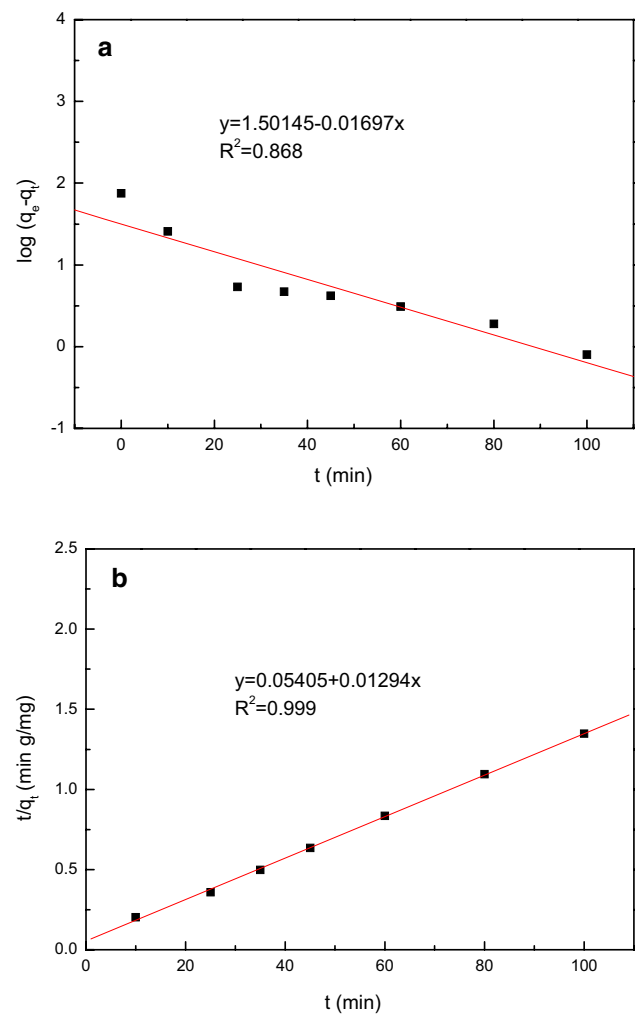
Fig. 7 Adsorption kinetic for MB adsorption onto 3D-HPGF nanocomposite adsorbent. **a** Pseudo-first-order model and **b** pseudo-second-order model

sites having equal adsorbate affinity, while the Freundlich isotherm model assumes heterogeneity of adsorption surfaces, which can be described by the following equations.

$$\frac{C_e}{q_e} = \frac{C_e}{q_{max}} + \frac{1}{k_L q_{max}} \tag{4}$$

$$\log q_e = \log k_F + \frac{1}{n} \log C_e \tag{5}$$

where C_e (mg/L) and q_e (mg/g) are the concentration and the adsorption capacity of MB dye at equilibrium, q_{max} (mg/g) is the maximum monolayer adsorption capacity, and k_L (L/mg) is the constant related to the energy of adsorption, which can be calculated by the slope and intercept of the linear plot C_e/q_e vs. C_e, respectively (in Fig. 8a). Meanwhile, k_F and $1/n$ are the Freundlich equilibrium constant

Table 1 Kinetic parameters for adsorption of MB dye onto 3D-HPGF nanocomposite adsorbent

Kinetic model	Parameters			
Pseudo-first-order	$q_{e,exp}$ (mg/g)	k_1 (min^{-1})	$q_{e,cal}$ (mg/g)	R^2
	69.6	0.0391	31.73	0.868
Pseudo-second-order	$q_{e,exp}$ (mg/g)	k_2 (min^{-1})	$q_{e,cal}$ (mg/g)	R^2
	69.6	0.0031	77.28	0.999
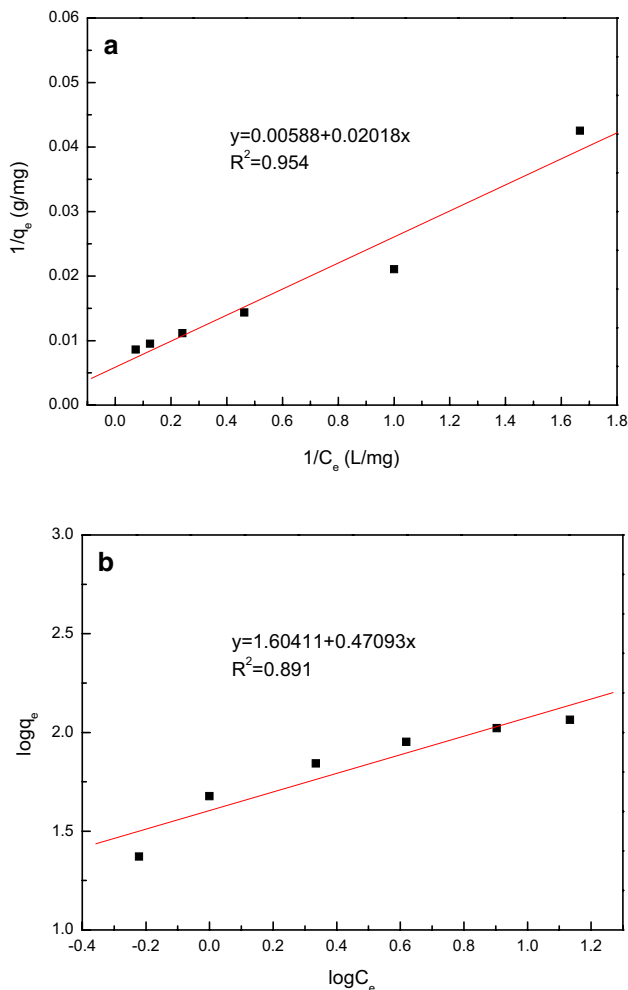
Fig. 8 Adsorption isotherms for MB adsorption onto 3D-HPGF nanocomposite adsorbent. **a** Langmuir isotherm and **b** Freundlich isotherm

and Freundlich adsorption constant, which can be calculated from intercept and slope of the linear plot between $\log C_e$ and $\log q_e$, respectively (in Fig. 8b). Based on the above isotherm models, the calculated parameters are listed in Table 2. It can be seen that the adsorption of MB dye onto 3D-HPGF nanocomposite adsorbent is better described by Langmuir isotherm model with higher correlation coefficients (R^2), which means the adsorption of MB dye onto 3D-HPGF nanocomposite adsorbent is a monolayer adsorption.

The thermodynamic studies provide in-depth information on inherent energetic changes that are associated with adsorption. The effect of temperature on MB dye adsorption onto the 3D-HPGF nanocomposite is investigated, and the related thermodynamic parameters are also calculated. The thermodynamic feasibility of the adsorbent-dye interaction process can be expressed by the following equations.

$$\Delta G^0 = -RT \ln K_d \qquad (6)$$

Here ΔG^0 is the change of the Gibbs free energy, R is the gas constant (8.3145 J/mol K), T is the temperature (K), K_d is the distribution coefficient ($K_d = q_e/C_e$). The related thermodynamic parameters are shown in Table 3. Obviously, the values of ΔG^0 are negative at different temperatures, suggesting the spontaneous nature of the process. Furthermore, the values of enthalpy change (ΔH^0) and entropy change (ΔS^0) associated with the processes are calculated using the following equations.

$$\ln K_d = \frac{\Delta S^0}{R} - \frac{\Delta H^0}{RT} \qquad (7)$$

The values of ΔS^0 and ΔH^0 can be calculated from the slope and intercept of van't Hoff plot ($\ln K_d$ vs. $1/T$), as shown in Fig. 9. The positive value of ΔH^0 indicates an

Table 2 Isotherm parameters for adsorption of MB dye onto 3D-HPGF nanocomposite adsorbent

Isotherm model	Parameters		
Langmuir	k_L (L/mg)	q_m (mg/g)	R^2
	0.2913	170.1	0.954
Freundlich	k_F (mg/g)	n	R^2
	40.19	2.12	0.891

Table 3 Adsorption thermodynamic parameters for MB dye adsorption onto 3D-HPGF nanocomposite adsorbent

ΔH^0 (kJ/mol)	ΔS^0 (J/mol K)	ΔG^0 (kJ/mol)		
		298 K	308 K	318 K
150.17	518.24	− 3.54	− 10.97	− 13.80

$$y = 62.32981 - 18.06077x$$
$$R^2 = 0.931$$
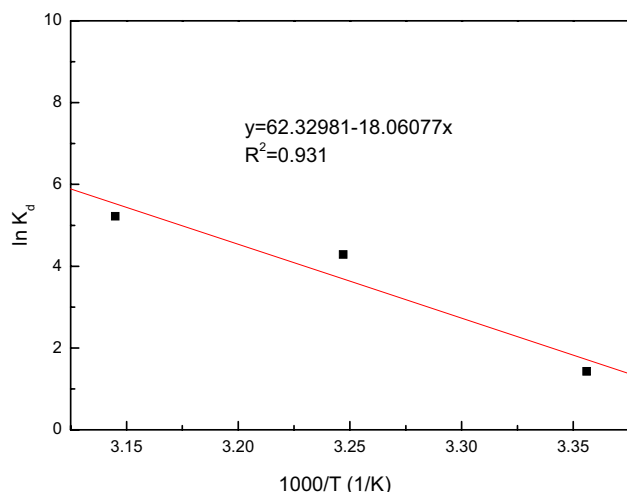
Fig. 9 Van't Hoff plot of ln K_d vs. 1/T (initial MB concentration: 30 mg/L; contact time: 45 min)
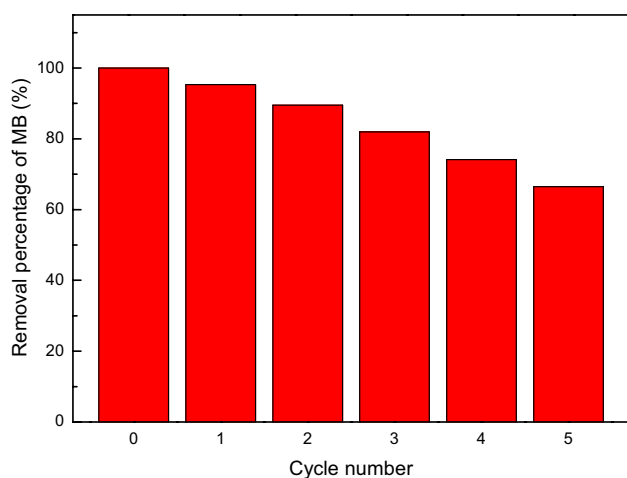
Fig. 10 Recycling of 3D-HPGF nanocomposite adsorbent after adsorbing MB dyes

endothermic nature of adsorption, while the positive value of ΔS^0 reflects an increase in randomness at the solid/solution interface during the adsorption process.

The regeneration ability of adsorbent is crucial for its practical application. The used 3D-HPGF nanocomposite can be regenerated simply by magnetic separation and treating with ethanol solution. As shown in Fig. 10, the recycling

of 3D-HPGF nanocomposite leads to a slight decrease of adsorption capacity. After the first and fifth recycle, the removal percentage of MB dye is 95.3 and 66.5%, respectively. These results indicate that 3D-HPGF nanocomposite adsorbent can be reused during practical applications.

4 Conclusions

In summary, three-dimensional hierarchical porous graphene–Fe_3O_4 nanocomposite has been successfully synthesized by a facile colloidal crystal templating method. The obtained 3D-HPGF nanocomposite has high specific surface area and three-dimensional hierarchical porous structures, which guarantee its adsorption performance for removing the dye contaminants from wastewater. The 3D-HPGF nanocomposite exhibits extraordinary removal capacity and fast adsorption rates for MB dye from aqueous solution, due to the van der Waals interactions occurring between hexagonally arrayed carbon atoms in the graphene sheet and the aromatic backbones of organic dye, and the strong π–π interactions between the benzene ring of organic dye and the large delocalized π-electron system of graphene. The kinetic study suggests the adsorption process follows pseudo-second-order kinetic model. The equilibrium data are well-modeled by Langmuir isotherm model. The thermodynamic parameters reveal that the adsorption process is spontaneous and endothermic in nature. Most importantly, 3D-HPGF nanocomposite adsorbent can be easily and efficiently regenerated for reuse. Therefore, the 3D-HPGF nanocomposite adsorbent can provide a better solution for solving the environmental problem of dye pollution in water resources due to its advantages of high adsorption capacity, fast adsorption rate, convenient magnetic separation and regeneration.

References

1. E. Forgacs, T. Cserhati, G. Oros, Removal of synthetic dyes from wastewaters: a review. Environ. Int. **30**, 953–971 (2004)
2. L. Sun, H.W. Yu, B.S. Fugetsu, Graphene oxide adsorption enhanced by in situ reduction with sodium hydrosulfite to remove acridine orange from aqueous solution, J. Hazard. Mater. **203–204**, 101–110 (2012)
3. H. Kim, A. Watthanaphanit, N. Saito, Simple solution plasma synthesis of hierarchical nanoporous MnO_2 for organic dye removal. ACS Sustain. Chem. Eng. **5**, 5842–5851 (2017)
4. L.Y. Zhang, X.R. Li, M.R. Wang, Y.J. He, L.Y. Chai, J.Y. Huang, H.Y. Wang, X.W. Wu, Y.K. Lai, Highly flexible and porous

nanoparticle-loaded films for dye removal by graphene oxide–fungus interaction. ACS Appl. Mater. Inter. **8**, 34638–34647 (2016)

5. N.M. Nursam, X.D. Wang, J.Z.Y. Tan, R.A. Caruso, Probing the effects of templating on the UV and visible light photocatalytic activity of porous nitrogen-modified titania monoliths for dye removal. ACS Appl. Mater. Inter. **8**, 17194–17204 (2016)

6. F. Fu, Q. Wang, Removal of heavy metal ions from wastewaters: a review. J. Environ. Manag. **92**, 407–418 (2011)

7. C. Sarkar, C. Bora, S.K. Dolui, Selective dye adsorption by pH modulation on amine-functionalized reduced graphene oxide–carbon nanotube hybrid. Ind. Eng. Chem. Res. **53**, 16148–16155 (2014)

8. P. Hadi, J.X. Guo, J. Barford, G. McKay, Multilayer dye adsorption in activated carbons–facile approach to exploit vacant sites and interlayer charge interaction. Environ. Sci. Technol. **50**, 5041–5049 (2016)

9. J.Y. Zhu, Y.M. Wang, J.D. Liu, Y.T. Zhang, Facile one-pot synthesis of novel spherical zeolite–reduced graphene oxide composites for cationic dye adsorption. Ind. Eng. Chem. Res. **53**, 13711–13717 (2014)

10. Y. Huang, X. Zheng, S.P. Feng, Z.Z. Guo, S. Liang, Enhancement of rhodamine B removal by modifying activated carbon developed from *Lythrum salicaria* L. with pyruvic acid. Colloid Surf. A **489**, 154–162 (2016)

11. P.K. Magdalena, G. Joanna, P. Robert, Removal of rhodamine B from water by modified carbon xerogels. Colloid Surf. A **543**, 109–117 (2018)

12. H. Wang, X.W. Huang, W. Li, J.F. Gao, H.G. Xue, R.K.Y. Li, Y.W. Mai, TiO_2 nanoparticle decorated carbon nanofibers for removal of organic dyes. Colloid Surf. A **549**, 205–211 (2018)

13. A. Kumar, P. Paul, S.K. Nataraj, Bionanomaterial scaffolds for effective removal of fluoride, chromium, and dye. ACS Sustain. Chem. Eng. **5**, 895–903 (2017)

14. X.F. Qin, F. Wang, S.H. Ren, L.X. Yang, Y.F. Meng, L.X. Sun, Self-forming salt-assisted synthesis of SiC nanoparticles and their adsorption property for methylene blue from aqueous solution. Ceram. Int. **42**, 847–852 (2016)

15. Q. Li, T. Yang, Q.F. Yang, F. Wang, K.C. Chou, X.M. Hou, Porous hexagonal boron nitride whiskers fabricated at low temperature for effective removal of organic pollutants from water. Ceram. Int. **42**, 8754–8762 (2016)

16. H. Yang, A. Sheikhi, T.G.M. van de Ven, Reusable green aerogels from cross-linked hairy nanocrystalline cellulose and modified chitosan for dye removal. Langmuir **32**, 11771–11779 (2016)

17. Y. Qin, L. Wang, C.W. Zhao, D. Chen, Y.H. Ma, W.T. Yang, Ammonium-functionalized hollow polymer particles as a pH-responsive adsorbent for selective removal of acid dye. ACS Appl. Mater. Inter. **8**, 16690–16698 (2016)

18. X.P. Wang, C. Hou, W. Qiu, Y.P. Ke, Q.C. Xu, X.Y. Liu, Y.H. Lin, Protein-directed synthesis of bifunctional adsorbent-catalytic hemin-graphene nanosheets for highly efficient removal of dye pollutants via synergistic adsorption and degradation. ACS Appl. Mater. Inter. **9**, 684–692 (2017)

19. J.L. Xiao, W.Y. Lv, Z. Xie, Y.Q. Tan, Y.H. Song, Q. Zheng, Environmentally friendly reduced graphene oxide as a broad-spectrum adsorbent for anionic and cationic dyes via pi-pi interactions. J. Mater. Chem. A **4**, 12126–12135 (2016)

20. G.Z. Kyzas, E.A. Deliyanni, D.N. Bikiaris, A.C. Mitropoulos, Graphene composites as dye adsorbents: review. Chem. Eng. Res. Des. **129**, 75–88 (2018)

21. J.L. Xiao, W.Y. Lv, Y.H. Song, Q. Zheng, Graphene/nanofiber aerogels: performance regulation towards multiple applications in dye adsorption and oil/water separation. Chem. Eng. J. **338**, 202–210 (2018)

22. J. Oliva, A.I. Martinez, A.I. Oliva, C.R. Garcia, A. Martinez-Luevanos, M. Garcia-Lobato, R. Ochoa-Valiente, A. Berlanga, Flexible graphene composites for removal of methylene blue dye-contaminant from water. Appl. Surf. Sci. **436**, 739–746 (2018)

23. K. Rathinam, S.P. Singh, Y.L. Li, R. Kasher, J.M. Tour, C.J. Arnusch, Polyimide derived laser-induced graphene as adsorbent for cationic and anionic dyes. Carbon **124**, 515–524 (2017)

24. K. Im, N.N. Duong, S. Kim, H.J. Kong, Y. Kim, C.S. Park, O.S. Kwon, H. Yoon, Graphene-embedded hydrogel nanofibers for detection and removal of aqueous-phase dyes. ACS Appl. Mater. Inter. **9**, 10768–10776 (2017)

25. A. Mahdizadeh, S. Farhadi, A. Zabardasti, Microwave-assisted rapid synthesis of graphene-analogue hexagonal boron nitride (h-BN) nanosheets and their application for the ultrafast and selective adsorption of cationic dyes from aqueous solutions. RSC Adv. **7**, 53984–53995 (2017)

26. H. Yan, X. Tao, Z. Yang, K. Li, H. Yang, A.M. Li, R.S. Cheng, Effects of the oxidation degree of graphene oxide on the adsorption of methylene blue. J. Hazard. Mater. **268**, 191–198 (2014)

27. N. Lu, G. He, J.X. Liu, G.H. Liu, J.T. Li, Combustion synthesis of graphene for water treatment. Ceram. Int. **44**, 2463–2469 (2018)

28. J.P. Zou, H.L. Liu, J.M. Luo, Q.J. Xing, H.M. Du, X.H. Jiang, X.B. Luo, S.L. Luo, S.L. Sui, Three-dimensional reduced graphene oxide coupled with Mn_3O_4 for highly efficient removal of Sb(III) and Sb(V) from water. ACS Appl. Mater. Interfaces **8**, 18140–18149 (2016)

29. J.J. Zhang, S.S. Fang, J.Y. Mei, G.P. Zheng, X.C. Zheng, X.X. Guan, High-efficiency removal of rhodamine B dye in water using g-C_3N_4 and TiO_2 co-hybridized 3D graphene aerogel composites. Sep. Purif. Technol. **194**, 96–103 (2018)

30. C. Xiang, R.H. Guo, J.W. Lan, S.X. Jiang, C. Wang, Z.F. Du, C. Cheng, Self-assembling porous 3D titanium dioxide-reduced graphene oxide aerogel for the tunable absorption of oleic acid and Rhodamine B dye. J. Alloy. Compd. **735**, 246–252 (2018)

31. C.Y. Hou, Q.H. Zhang, Y.G. Li, H.Z. Wang, P25–graphene hydrogels: room-temperature synthesis and application for removal of methylene blue from aqueous solution. J. Hazard. Mater. **205–206**, 229–235 (2012)

32. C.Y. Liu, H.Y. Liu, A.R. Xu, K.Y. Tang, Y. Huang, C. Lu, In situ reduced and assembled three-dimensional graphene aerogel for efficient dye removal. J. Alloy Compd. **714**, 522–529 (2017)

33. Y.C. Shi, A.J. Wang, A.J. Wang, X.L. Wu, J.R. Chen, J.J. Feng, Green-assembly of three-dimensional porous graphene hydrogels for efficient removal of organic dyes. J. Colloid Interf. Sci. **484**, 254–262 (2016)

34. R. Guo, T.F. Jiao, R.F. Li, Y. Chen, W.C. Guo, L.X. Zhang, J.X. Zhou, Q.R. Zhang, Q.M. Peng, Sandwiched Fe_3O_4/carboxylate graphene oxide nanostructures constructed by layer-by-layer assembly for highly efficient and magnetically recyclable dye removal. ACS Sustain. Chem. Eng. **6**, 1279–1288 (2018)

35. L.Y. Zhang, W.L. Zhang, Z.Q. Zhou, C.M. Li, γ-Fe_2O_3 nanocrystals-anchored macro/meso-porous graphene as a highly efficient adsorbent toward removal of methylene blue. J. Colloid Interf. Sci. **476**, 200–205 (2016)

36. E.M. Sakho, S. Thomas, N. Kalarikkal, O.S. Oluwafemi, Dielectric and dye adsorption properties of luminescent-superparamagnetic MFe_2O_4 (M = Mn, Mg)/reduced graphene oxide composites. Ceram. Int. **44**, 3904–3914 (2018)

37. W. Wang, Y.L. Cheng, T. Kong, G.S. Cheng, Iron nanoparticles decoration onto three-dimensional graphene for rapid and efficient degradation of azo dye. J. Hazard. Mater. **299**, 50–58 (2015)

38. B. Mu, J. Tang, L. Zhang, A.Q. Wang, Facile fabrication of superparamagnetic graphene/polyaniline/Fe_3O_4 nanocomposites for fast magnetic separation and efficient removal of dye. Sci. Rep. **7**, 5347 (2017)

39. T.K. Sahu, S. Arora, A. Banik, P.K. Iyer, M. Qureshi, Efficient and rapid removal of environmental malignant arsenic(III) and industrial dyes using reusable, recoverable ternary iron oxide-ormosil-reduced graphene oxide composite. ACS Sustain. Chem. Eng. **5**, 5912–5921 (2017)

40. Y.R. Liu, Z.Q. Zhang, T.Y. Wang, Enhanced hydrogen storage performance of three-dimensional hierarchical porous graphene with nickel nanoparticles. Int. J. Hydrog. Energy **43**, 11120–11131 (2018)

41. V.H. Pham, T.T. Dang, S.H. Hur, E.J. Kim, J.S. Chung, Highly conductive poly(methyl methacrylate) (PMMA)-reduced graphene oxide composite prepared by self-assembly of PMMA latex and graphene oxide through electrostatic interaction. ACS Appl. Mater. Inter. **4**, 2630–2636 (2012)

42. R.C. Schroden, M. Al-Daous, S. Sokolov, B.J. Melde, J.C. Lytle, A. Stein, M.C. Carbajo, J.T. Fernándezb, E.E. Rodríguezj, Hybrid macroporous materials for heavy metal ion adsorption. J. Mater. Chem. **12**, 3261–3267 (2002)

43. M. Zhang, D. Lei, X. Yin, L. Chen, Q. Li, Y. Wang, T. Wang, Magnetite/graphene composites: microwave irradiation synthesis and enhanced cycling and rate performances for lithium ion batteries. J. Mater. Chem. **20**, 5538–5543 (2010)

44. J. Zhao, S. Pei, W. Ren, L. Gao, H.M. Cheng, Efficient preparation of large-area graphene oxide sheets for transparent conductive films. ACS Nano **4**, 5245–5252 (2010)

45. S. Pei, J. Zhao, J. Du, W. Ren, H.M. Cheng, Direct reduction of graphene oxide films into highly conductive and flexible graphene films by hydrohalic acids. Carbon **48**, 4466–4474 (2010)

46. Y. Xue, H. Chen, D. Yu, S. Wang, M. Yardeni, Q. Dai, M. Guo, Y. Liu, F. Lu, J. Qu, L. Dai, Oxidizing metal ions with graphene oxide: the in situ formation of magnetic nanoparticles on self-reduced graphene sheets for multifunctional applications. Chem. Commun. **47**, 11689–11691 (2011)

47. S. Adireddy, C.K. Lin, V. Palshin, Y.M. Dong, R. Cole, G. Caruntu, Size-controlled synthesis of quasi-monodisperse transition-metal ferrite nanocrystals in fatty alcohol solutions. J. Phys. Chem. C **113**, 20800–20811 (2009)

48. Y. Huang, A.A. Keller, Magnetic nanoparticle adsorbents for emerging organic contaminants. ACS Sustain. Chem. Eng. **1**, 731–736 (2013)

49. F.H. Li, Y. Bao, J. Chai, Q.X. Zhang, D.X. Han, L. Niu, Synthesis and application of widely soluble graphene sheets. Langmuir **26**, 12314–12320 (2010)